

DEM of triaxial tests on crushable cemented sand

J. P. de Bono · G. R. McDowell · D. Wanatowski

Received: 5 February 2014 / Published online: 30 April 2014
© Springer-Verlag Berlin Heidelberg 2014

Abstract Using the discrete element method, triaxial simulations of cemented sand consisting of crushable particles are presented. The triaxial model used features a flexible membrane, allowing realistic deformation to occur, and cementation is modelled using inter-particle bonds. The effects of particle crushing are explored, as is the influence of cementation on the behaviour of the soil. An insight to the effects that cementation has on the degree of crushing is presented.

Keywords Discrete-element modelling · DEM · Particle crushing · Cemented Sand

1 Introduction

The behaviour of cemented sand has been given much attention over recent years, and has been the subject of a number of laboratory studies. The presence of cement has a dramatic influence on the triaxial behaviour of sand; for a sand sheared at a given confining pressure, cementation (either natural or artificial) generally causes an increase in stiffness, peak strength, and the amount and rate of dilation; with these effects increasing with cement content [1–3]. The addition of cement introduces well-defined yield points and peak stresses, and reduces the axial strain at the peak stress. Cementation also influences the failure modes of the sand; brittle failure with shear planes are often witnessed in cemented specimens, while barrelling failure is observed for equivalent uncemented samples at the same confining pressure [4–6].

Particle crushing, while a separate phenomenon, also largely affects the stress and strain behaviour of granular soils. In triaxial tests, particle breakage decreases the rate of dilation [7], which in turn has an influence on any peak stress associated with the density. The degree of crushing is influenced by a number of factors, most principally the strength of the grains and the effective stress state; as such the effects of particle crushing are most pronounced at high pressures [8].

The discrete element method (DEM) has proved to be a useful tool for modelling granular soil; however, much of currently available literature using DEM to model cemented sand has been limited to two dimensions, for example [9–13]. Potyondy and Cundall [14] included some three dimensional modelling, although their work didn't feature flexible boundaries which are characteristic of laboratory triaxial tests. Wang and Tonon [15] however, did use flexible boundaries when modelling rock, although the focus of their work was to highlight the advantages and importance of such boundaries, rather than the micro mechanics of inter particle bonding.

Particle crushing is often ignored in DEM, due to difficulties in implementing an effective *and* realistic breakage mechanism. In recent years, crushable particles have been modelled using DEM either by using agglomerates ('grains' consisting of smaller elementary spheres, bonded together), or by replacing 'broken' particles with smaller, self-similar fragments. Using the former method, Bolton et al. [16] showed that crushable particles are necessary for achieving realistic levels of volumetric contraction when modelling triaxial shear tests on granular soils. However, one drawback with using agglomerates is the large number of elementary particles required, which severely limits the overall number of grains that can be used; Bolton et al. [16] used just 389 agglomerates, consisting of less than 50 spheres each, while Lim and McDowell [17] showed that each agglomerate ide-

J. P. de Bono · G. R. McDowell (✉) · D. Wanatowski
University of Nottingham, Nottingham, UK
e-mail: glenn.mcdowell@nottingham.ac.uk

ally should comprise at least 500 spheres to correct capture the size effect on strength.

The following work aims to show that is possible to model three-dimensional triaxial simulations on a crushable, cemented sand using DEM, with a large number of particles. The work presented here features a triaxial model with a flexible membrane allowing realistic deformation [18], with a simple breakage mechanism incorporated that replaces broken sand particles with new, smaller fragments [19], and follows on from the authors' recent work investigating the behaviour of a cemented sand with crushable particles in normal compression [20]. This paper aims to investigate the combined effects of cement bond breakage and particle crushing in triaxial shear, and provide a step towards improving the realism of DEM simulations.

2 Triaxial model

2.1 Specimen

The sand particles are modelled using spheres; the triaxial sample used is cylindrical, with a height of 100 mm and a diameter of 50 mm. The sand particles use the Hertz–Mindlin contact model, and are given a Poisson's ratio, $\nu = 0.25$ and a shear modulus, $G = 28$ GPa, typical values for quartz. The initial specimen is mono-disperse, consisting of 3,350 particles of uniform size $d_0 = 4$ mm, and is generated using the radii expansion method [21] to give an initial voids ratio $e_0 = 0.75$. Although this quantity of particles may be considered unrealistic, it is a larger number than used in many of the similar simulations of cemented materials [12, 13] or crushable soils [16, 22]. Furthermore, the particles can break an unlimited number of times, giving a higher 'breakage capacity' than the agglomerates used in the aforementioned studies. This initial diameter (which determines how many specimen particles are created) was chosen for computational efficiency; using a smaller initial diameter would result in a much larger number of both specimen particles and membrane particles (which are required to be smaller). Although this may seem somewhat unrealistic, this work serves as a fundamental investigation in to the combined effects of crushing and cementation, rather than a direct physical calibration.

2.2 Membrane

The flexible membrane used is the same as described in de Bono et al. [18], full details of which won't be repeated, the only principal difference being that the Hertz–Mindlin contact model is now used, rather than the linear spring model. To summarise, the cylindrical membrane consists of hexagonally-arranged particles, which are created a factor of 1/3 smaller than the smallest specimen particle. These parti-

cles are given artificially high stiffness—both to prevent them from penetrating the specimen, and to keep them aligned; with a system in place to remove the additional hoop tension which resulted. In the previous work, the membrane particles were bonded using contact bonds, which were vanishingly small and transmitted no moments. In this work however, due to the different contact model used (Hertz–Mindlin), membrane particles are ascribed a Poisson's ratio $\nu = 0.5$ (typical for rubber) and given an arbitrarily high shear modulus of $G = 1$ MPa to prevent penetration. The membrane particles are bonded together with parallel bonds [21], the diameter of which are 10^{-10} times smaller than the membrane particles. These bonds are given 'stiffnesses' (stress per displacement) of 1×10^{40} Pa/m; sufficient to keep the membrane particles aligned. The excess hoop tension is alleviated by allowing the membrane particles to expand, details of which are in de Bono et al. [18].

2.3 Particle crushing

Crushing has generally been modelled using DEM via two alternatives: replacing 'breaking' grains with new, smaller fragments, generally in two-dimensions [23–27] or by using three-dimensional agglomerates [16, 22, 28, 29]. In the latter method, no consideration was given to the complex distribution of loads on each particle at its multiple contacts; however, McDowell and de Bono [19] allowed three-dimensional particles to fracture without the use of agglomerates by considering the stresses induced in a particle due to the multiple contacts. The same breakage mechanism and criteria are used in the following simulations, in which each particle is allowed to split into two new fragments, when the value of induced particle stress is found to be greater or equal to its strength. The new sphere fragments overlap enough to be contained within the bounding parent sphere, with the axis joining the new spheres aligned in the direction of the minor principal stress (Fig. 1). Although the fragments of broken spheres are not spheres, realistic particle shape has *not* been employed in this work—however, Bowman et al. [30] demonstrated (using Fourier descriptor analysis) that crushing a laboratory-grade silica sand resulted in statistically-*insignificant* changes in particle elongation and shape, suggesting that using self-similar fragments in these simulations is acceptable. The total volume of the new spheres is equal to that of the original parent sphere, obeying conservation of mass. This produces local pressure spikes during breakage; however the fragments move along the direction of the minor principal stress for the original particle, just as would occur for a single particle crushed between platens. Although conservation of energy is not observed in this case, the goal is to achieve an effective breakage mechanism as simple and effective as possible. As several authors (e.g. [23]) have implied, it is not possible to simulate *perfectly* realistic fracture using self-similar frag-

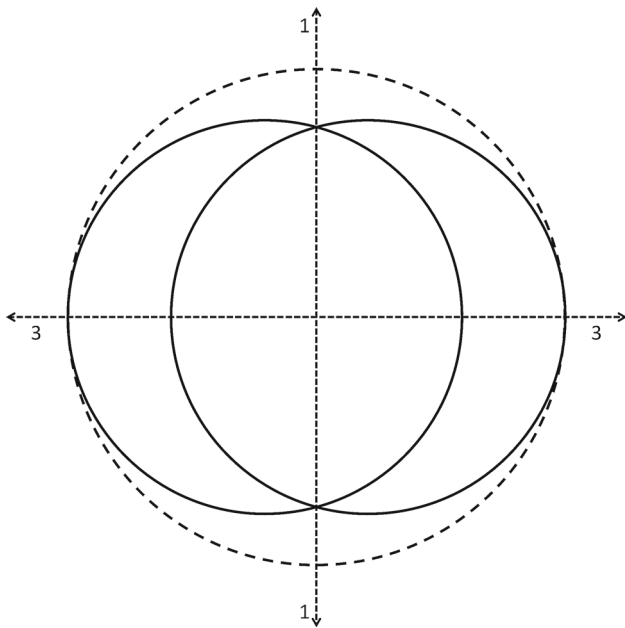


Fig. 1 Equal diametral splitting mechanism

ments; however it is not the purpose of this study to resolve this problem, but rather to adopt the best approach to investigate the effects of cementation and particle crushing during shear.

McDowell and de Bono [19] showed that the octahedral shear stress, q within a particle, given by:

$$q = \frac{1}{3} \left[(\sigma_1 - \sigma_2)^2 + (\sigma_2 - \sigma_3)^2 + (\sigma_1 - \sigma_3)^2 \right]^{1/2} \quad (1)$$

could be used to determine whether fracture should occur or not.

Jaeger [31] proposed the tensile strength of grains could be measured by diametral compression between platens as $\sigma = F/d^2$. In PFC3D, for a sphere of size d compressed between two walls exerting force F , the value of induced octahedral shear stress, q , was found to be:

$$q = 0.9 \frac{F}{d^2} \quad (2)$$

and so proportional to the assumed induced stress in particle crushing tests. The octahedral shear stress was deemed an appropriate means by which to determine fracture, as it takes into account multiple contacts and complex distribution of loads while avoiding the use of agglomerates.

By crushing individual sand particles, McDowell et al. [32, 33] showed that the stresses at failure for a given particle size satisfied a Weibull distribution of strengths (with same variation regardless of size). The mean strength σ_m of the particles was related to size by $\sigma_m = d^{-b}$ (where b describes the size-hardening law). Hence McDowell and de Bono [19]

assumed a particle would break when the *octahedral shear stress* was greater than or equal to its strength, where the strengths of the particles satisfy a Weibull distribution of q values. The strengths were related to size by:

$$q_0 \propto d^{-b} \quad (3)$$

which, assuming that the Weibull size effect is applicable to soil particles [33], leads to:

$$q_0 \propto d^{-3/m} \quad (4)$$

where q_0 is the characteristic strength, and is a value of the distribution such that 37% (i.e. $\exp[-1]$) of random strengths are greater—and is related to the mean; m is the modulus, which describes the variation of the distribution.

Particle breakage is determined using the octahedral shear stress according to equation (1). The particles in the simulations have random strengths from a distribution defined by the Weibull parameters obtained from silica sand by McDowell [34], i.e. $q_0 = 20$ MPa for the initial particles ($d_0 = 4$ mm); the Weibull modulus, $m = 3.3$; and the size-hardening law is governed by equation (4), which is used to attribute random strengths to new fragments. The details of the specimen and membrane used in the following simulations are given in Table 1.

2.4 Cementation

Cement bonds are modelled using the parallel bond feature of the software [21]. These consist of a finite-sized cylindrical piece of material between the two particles, acting in parallel with the standard force-displacement contact model. These have been used in previous studies to model structured soils, e.g. [11, 13, 14]; as well as by the authors [20, 35] in modelling cemented sand. The bonds are defined by normal and shear stiffness (in terms of stress/displacement), normal and shear strength (in terms of stress) and size, and are installed before application of the confining pressure.

It is somewhat unclear how to simulate the size of cement bonds; one may consider them small relative to the particles, occurring just at the contacts and independent of particle size; or as proportional to the particle diameters, filling much of the void space. Both of these approaches seem acceptable depending on interpretation and analysis of images; in this paper, all bonds are created with the same size, equal to the sand particles ($d_{bond} = d_0$). To reduce the number of variables, and because this paper is *not* specifically concerned with calibration against physical tests, the parallel bond normal and shear stiffnesses are set equal to one another to minimise input variables, as are the mean normal and shear strengths. The parallel bond normal stiffness is defined assuming that cement has an elastic modulus of

Table 1 Summary of DEM parameters for triaxial model

<i>Triaxial sample properties</i>	
Size: height × diameter (mm)	100 × 50
No. of particles	3,350
Particle friction coefficient	0.5
Contact model	Hertz–Mindlin
Shear modulus, G (GPa)	28
Poisson's ratio, ν	0.25
Density (kg/m^3)	2650
Coefficient of uniformity, C_u	1.0
Particle diameter, d_0 (mm)	4.0
Voids ratio, e_0	0.75
37% Strength, q_0 (MPa)	20.0 (for $d = d_0$)
Weibull modulus, m	3.3
Wall Friction Coefficient	0
Parallel bond diameter (mm)	4.0
Parallel bond stiffness (Pa/m)	7.5×10^{12}
Parallel bond 37% Strength (MPa)	10
<i>Triaxial membrane properties</i>	
No. of particles	3224
Friction coefficient	0
Contact model	Hertz–Mindlin
Shear modulus, G (GPa)	1
Poisson's ratio, ν	0.5
Density (kg/m^3)	1000
Particle diameter, d_0 (mm)	2.66
Parallel bond diameter (mm)	2.66×10^{-10}
Parallel bond stiffness (Pa/m)	1×10^{40}
Parallel bond strength (Pa)	1×10^{30}

around 30 GPa [36] and bonds are given random values from a distribution of strengths. De Bono et al. [20,35] showed that a Weibull distribution of strengths with a modulus of 0.5 was appropriate for modelling Portland cement, hence the parallel bond strengths here satisfy a Weibull distribution with a modulus of 0.5, with an arbitrary characteristic strength of 10 MPa.

With regard to simulating an increasing degree of cementation, analysis of experimental data could suggest altering the variation or magnitude of bond strengths and stiffness, or various combinations thereof, while analysing high magnification images would suggest altering the quantity of bonds and/or bond size. It was demonstrated and justified in related work by the authors [20]—and will also be shown here—that increasing the *quantity* of parallel bonds is the single most effective method of capturing the correct qualitative change in behaviour that results from an increase in cement content. Increasing the strength or stiffness of bonds fails to capture *all* the qualitative effects one would expect with an increase

in cement content. By default, when parallel bonds are created, they are installed at existing particle contacts, as well as between particles within *very* close proximity. By increasing this proximity in which non-touching particles are bonded to one another, an increasing quantity of parallel bonds can be installed. Hence, an increasing degree of cementation (i.e. cement content) is modelled herein by installing a larger number of bonds, and is measured by the average number of parallel bonds per particle.

2.5 Procedure

For the particle breakage mechanism described (used previously in [19,20,37,38]), particles are only allowed to break at *discrete intervals*, with a number of computational timesteps allowed between these breakages to allow the elastic energy from the overlaps to dissipate. The same approach is therefore adopted for bond breakage, i.e. the inter-particle bonds (cement) are only allowed to break at given intervals. This is following the authors' recent work on modelling the behaviour of crushable cemented sand in compression [20]; the complementary work presented here investigating the behaviour during triaxial shear.

The simulations are strain controlled; i.e. the top platen is accelerated downwards, then decelerated and stopped after an increase in axial strain of 0.01%. During application of the confining pressure, and then immediately following each strain increment, the cemented sand particles are checked and if the normal or shear stress at any contact exceeds the strength of the cement bond (*if* one is present), then the bond is considered broken and removed. After the all the contacts have been checked and the bonds allowed to break, the stresses *within* the particles are checked and the particle themselves allowed to break. A number of timesteps (inversely proportional to the *size* of the numerical timestep) are then completed, over the course of which *no* bonds or particles may break; this is to allow the artificial energy from new overlapping particles to dissipate. These two processes are repeated (allowing fragments to break multiple times if necessary) until no further breakages occur; after which the next strain increment is applied.

With regard to the influence that cementation (i.e. particle bonding) has on particle crushing, there is no conclusive evidence available in the literature. Coop and Atkinson [1] suggested that bond breakage precedes or coincides with particle breakage—however; by default, in the simulations particles may break regardless of whether they are bonded or not. Additionally, if a particle breaks, any bonds associated with it are automatically removed when the 'broken' particle is deleted and replaced by new fragments. It is generally believed that during normal compression, cementation reduces particle crushing (e.g. [6]), based on the observation that increasing the cement content of sand reduces

the compressibility. This proposition seems feasible if one envisages a sand particle bonded by cement to neighbouring particles—the cement will increase the contact which area, which would reduce the induced tensile stress [31]. When modelling crushable cemented sand, de Bono and McDowell [20] investigated various configurations of bond and particle breakage, and it was found that if the presence of cementation *prevented* particles from fracturing, good qualitative agreement could be observed with experiments, and cementation resulted in a reduction of particle crushing. This method is adopted here, and is achieved by simply *not* allowing any particle to break if there exists one or more parallel bonds attached to it, meaning bond breakage *must precede* particle breakage. This approach is reasonable if one considers a particle coated in cement, or heavily bonded—for the particle to be loaded diametrically—which will give the highest octahedral shear stress—then the cementation will *have* to be broken first.

The triaxial test variables monitored and recorded during the simulations are the deviatoric stress, q , the axial strain, ε_a , and volumetric strain, ε_v . The deviatoric stress is measured as the difference between the axial stress (the major principal stress) and confining pressure (minor principal stress), where the axial stress is obtained from the average stress acting on the top and bottom platens. The volumetric strain is calculated using the current and original volumes of the sample; the volume of the sample being calculated from the locations of the membrane particles [18].

3 Cemented sand

Experimental data for triaxial tests on sand bonded with various quantities of Portland cement are shown in Fig. 2 from Marri et al. [6]. The figure shows graphs of deviatoric stress, stress ratio and volumetric strain plotted against axial strain, for Portaway sand bonded with various amounts of Portland cement (measured by percentage dry mass), sheared under a confining pressure of 1 MPa. The figure shows that the addition of cement causes a peak stress to occur and increases the overall dilation. Increasing the amount of cement magnifies these effects—by causing the peak stress to increase and become more distinguished, and reducing the strain at this stress. In general, increasing the cement content causes the behaviour to become more brittle.

Figure 3 shows the equivalent set of results from simulations of a crushable sand, sheared under 1 MPa of confining pressure, with varying levels of bonding. An increasing degree of cementation is modelled by increasing the quantity of bonds within the material, measured by the average number of parallel bonds per particles. The figure shows the deviatoric stress, stress ratio and volumetric strain as a function of axial strain for simulations with an average of 0 (unbonded),

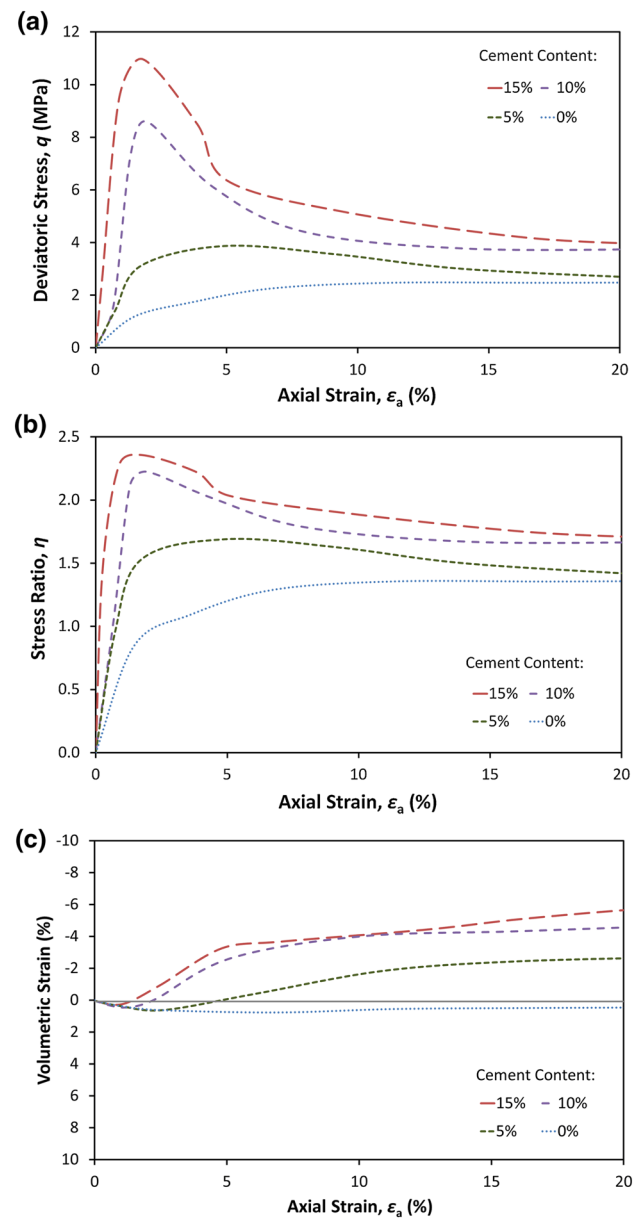


Fig. 2 Experimental triaxial results for sand at 1 MPa confining pressure with a range of Portland cement contents: deviatoric stress (a), stress ratio (b) and volumetric response (c), versus strain [6]

5, 10 and 15 parallel bonds per particle. All four simulations start with an initially mono-disperse material ($d_0 = 4$ mm), and as mentioned above, bond breakage must precede particle crushing.

The results show the correct trend that one would expect from an increase in cement content: there is an increase in the peak and maximum deviatoric stress, a higher initial stiffness and there is a more dilative response; in general the material displays more brittle stress–strain behaviour. The peak deviatoric stress appears to occur at slightly earlier axial strains with an increasing degree of cementation, in harmony with typical experimental results such as

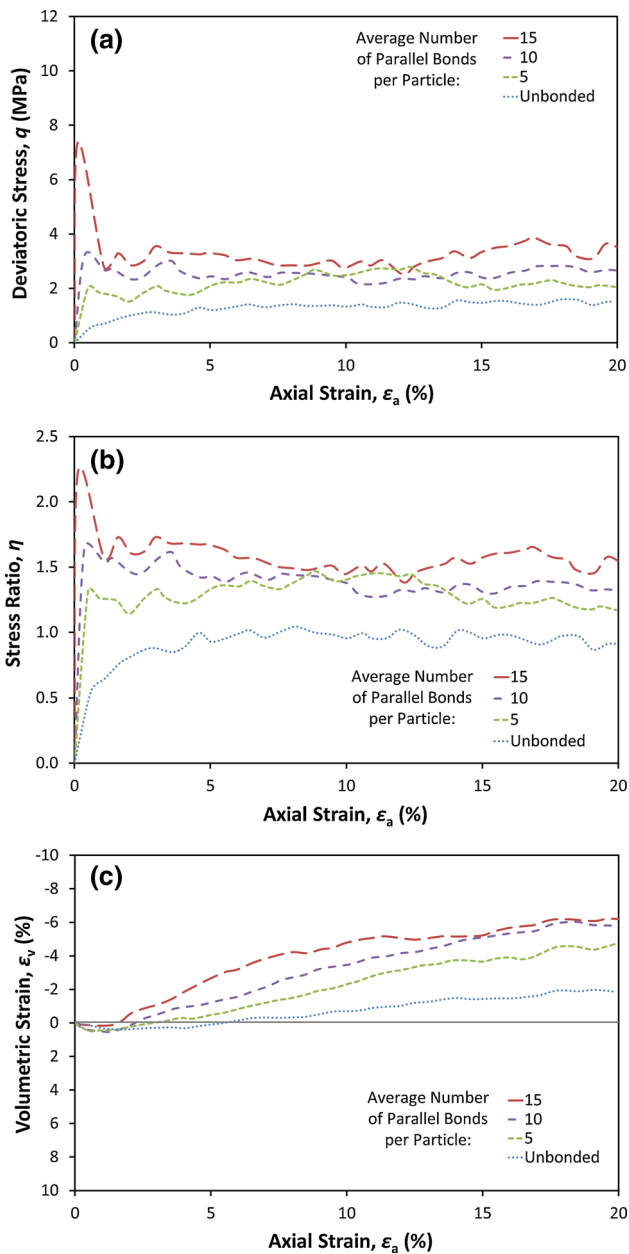


Fig. 3 Triaxial results for simulations of crushable sand with an increasing degree of cementation: deviatoric stress (a), stress ratio (b) and volumetric response (c) versus strain

those shown in Fig. 2. The deviatoric stress responses do not appear to completely converge at large strains, displaying agreement with the experimental results, which also do not converge, even at strains as high as 30%. Both numerical and experimental stress ratio graphs display the same pattern of behaviour, and reveal slightly different final values of η for the various materials. The most heavily cemented samples display the highest final stress ratios, suggesting that there is still active cementation, affecting the macroscopic grading at high strains under such a confining pressure. This is confirmed by the quantity of intact parallel bonds: at the

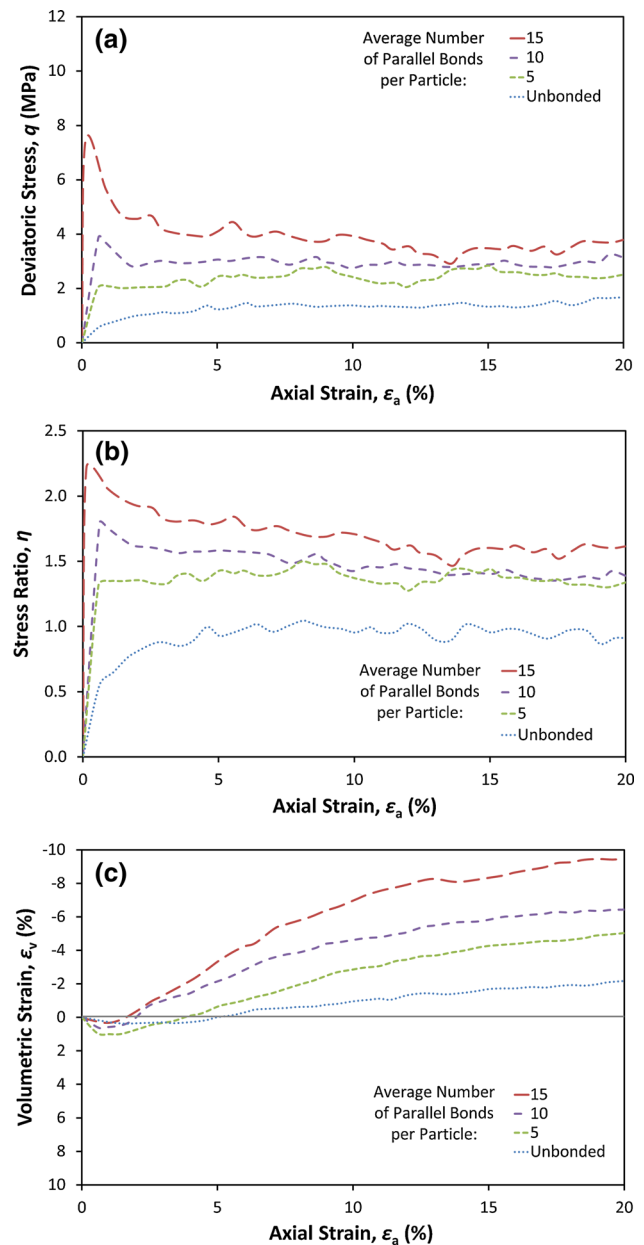


Fig. 4 Triaxial results for simulations of non-crushable sand with an increasing degree of cementation: deviatoric stress (a), stress ratio (b) and volumetric response (c) versus strain

end point of the simulations (i.e. $\epsilon_a = 20\%$), the lightly, medium, and heavily cemented simulations had 1,029, 1,262 and 1,738 parallel bonds remaining respectively. Repeating the tests with a higher confining pressure would be expected to reduce the difference in the final values of stress ratio.

Figure 4 shows the corresponding results for simulations using unbreakable particles. The stress–strain behaviour is largely the same as above, with the introduction of cement producing the same results: an increase in peak/maximum deviatoric stress, higher initial stiffness and increased dilation; with these effects increasing with cement content. The unbreakable simulations however appear to display very

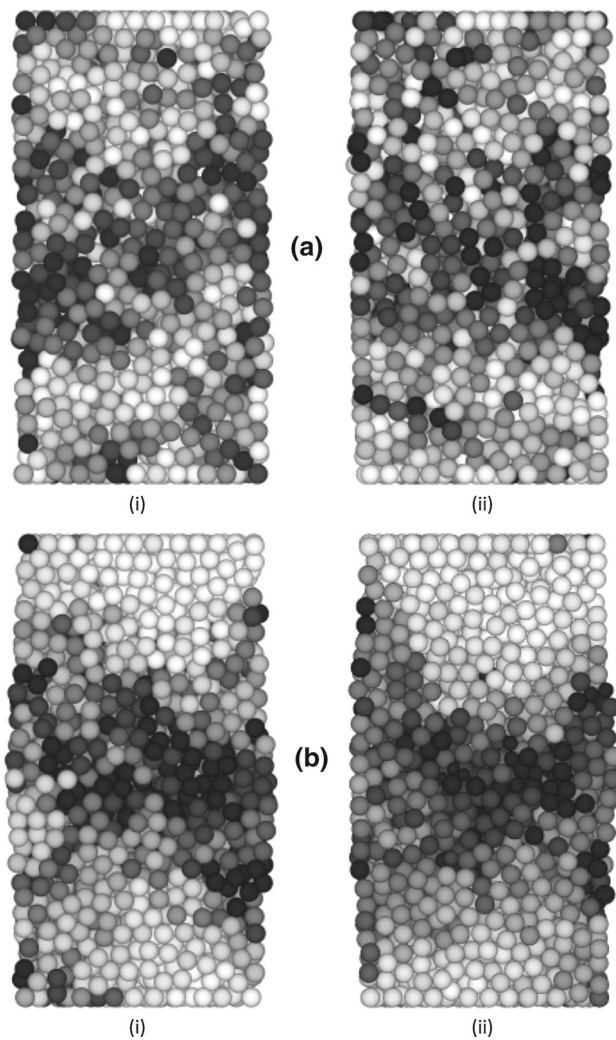
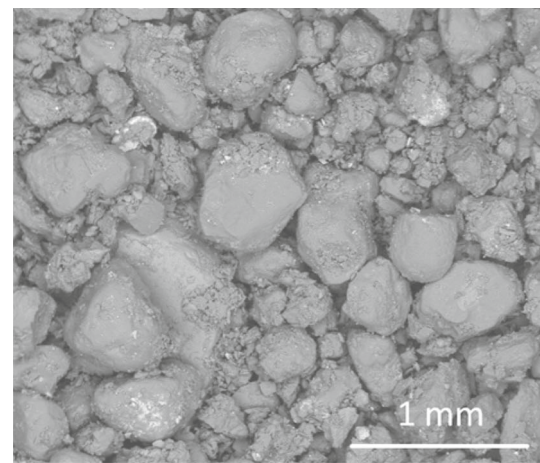


Fig. 5 Particle rotations on a vertical cutting plane through the samples, at 4 % axial strain: unbonded simulations (a) and heavily cemented simulations (b), with unbreakable particles (i) and breakable particles (ii). *Dark* indicates the most rotation

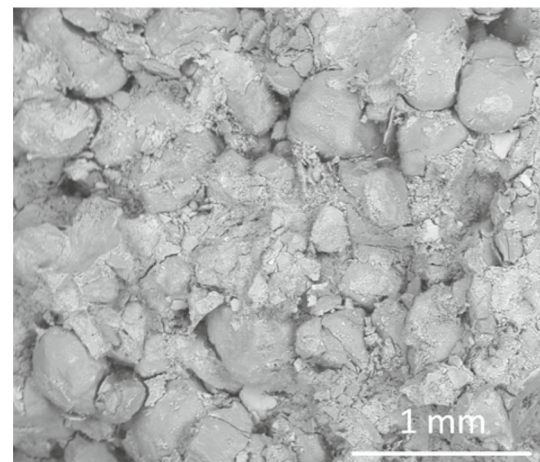
slightly higher values of peak stress and dilation. This is because as particles are unable to break in these simulations, they will need to rearrange to accommodate the macroscopic strain by sliding and rolling over one another (as opposed to breaking), requiring additional dilation. However, the difference is slight, and if smaller, more realistic initial particles were used, one would expect there to be even less difference between the crushable and non-crushable simulations—due to the smaller particles being stronger and therefore less likely to break.

At the end of these simulations (20 % axial strain), the quantities of intact bonds are 1,048, 1,352, and 1,682, respectively for the lightly, medium and heavily cemented non-crushable materials; similar to the crushable cemented sand simulations above.

Increasing the cement content (by increasing the quantity of parallel bonds) causes the material to become more brittle;



(a)



(b)

Fig. 6 Photographs showing close-ups of uncemented sand (a) and cemented sand (b) after drained triaxial shearing, under 20 MPa confining pressure [6]

this is also evident in the deformation. Figure 5 displays the particle rotations on a vertical cutting plane at approximately 4 % axial strain (around the point of maximum dilation). The rotations are given for the unbonded and most heavily bonded simulations, for both crushable *and* non-crushable simulations. Both unbonded simulations in Fig. 5a display no clear pattern, while the heavily cemented simulations in Fig. 5b display localised failure with mild shear planes. This indicates that the ability for particles to crush has little effect on the failure mode and the overall deformation of cemented sand.

Marri et al. [6] analysed particle breakage resulting from their high-pressure triaxial tests on cemented and uncemented sand. They provided photographic images of samples after shearing to approximately 30 % axial strain, key examples of which are given in Fig. 6. The two images compare an uncemented sample of sand (a) and a sample with 15 % content of Portland cement (b); both sheared under a confin-

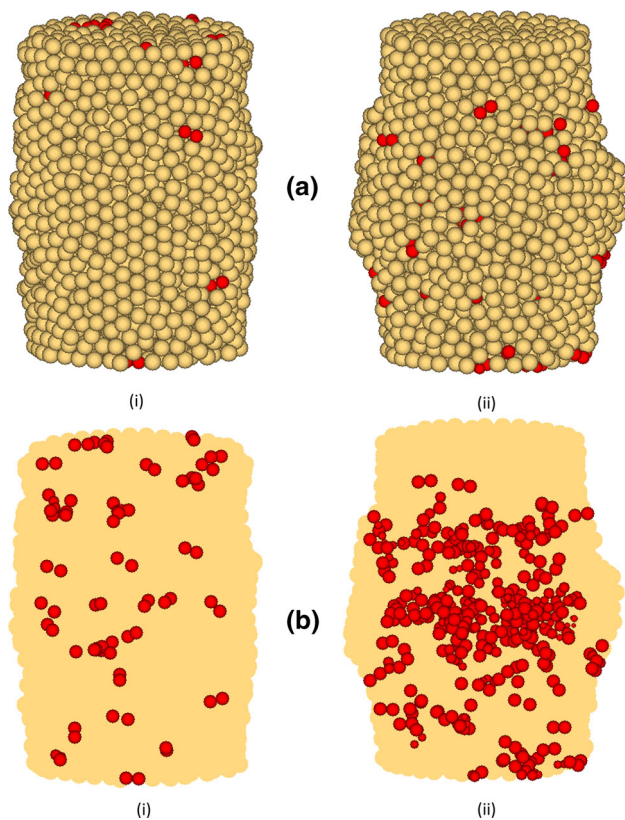


Fig. 7 External views of the samples with the broken fragments highlighted (a), and inner views showing all broken fragments (b); for the unbonded simulation (i) and heavily cemented (ii)

ing pressure of 20 MPa. Marri et al. [6] suggested that the amount of particle crushing appeared less in the cemented soil—although this can be disputed, as both images clearly reveal what appear to be broken particles. Furthermore, in the case of the cemented sand, the cementation obscures the particles, which may conceal further particle breakage.

With regards to the *crushable* simulations, the unbonded and most heavily cemented samples (with an average of 0 and 15 bonds per particle respectively) sheared under 1 MPa confining pressure are shown in Fig. 7a, after shearing to 20% axial strain. Although the broken fragments are highlighted, no major differences with regards to the amount of crushing are *externally* visible. However, the cemented material has experienced a total of 244 breakages. Overall, 140 original particles have undergone fragmentation, meaning 4.18% by mass has crushed. This is markedly more crushing than the unbonded specimen, in which only 1.13% of the sample has broken at the same stage. These numbers can be confirmed visually in Fig. 7b, which presents similar images of the samples, but reveal the inner breakages. These latter images also reveal a small number of significantly smaller particles in the heavily cemented material—indicating that some fragments have broken repeatedly; a phenomenon which is not observed in the uncemented sample.

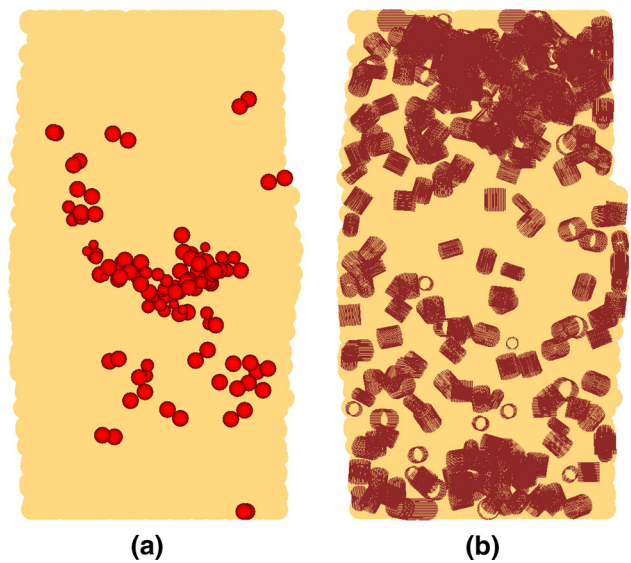


Fig. 8 Images of the heavily cemented, crushable sample after 4% axial strain. Inner view with all broken fragments highlighted (a), and view of the remaining intact parallel bonds on a vertical cutting plane (b)

Considering just the heavily cemented sample, the broken fragments are shown again in Fig. 8a, in which a horizontal view at 4% axial strain is presented (all fragments are displayed, throughout the sample), taken from the same angle as Fig. 5b, ii. The crushing does not appear to occur uniformly throughout the sample, rather it appears very localised. The fragments indicate a shear plane, in harmony with the Fig. 5b, ii, which displays the particle rotations from an identical point of view. Again, from this same point of view, Fig. 8b shows the remaining unbroken parallel bonds at the same axial strain (for clarity, only bonds on a vertical cutting plane through the centre of the sample are displayed). Most bond breakages have occurred in the same area as crushing, which is unsurprising considering bond breakage must *precede* particle fragmentation. Particle crushing, bond breakage and the particle rotations all conform to the same shear plane, showing that the deformation and failure is brittle, and highly localised. At the same strain, the uncemented simulation has experienced only 8 breakages.

Therefore, by using the intrusive capability of DEM, the simulations suggest that the presence of cement—contrary to what Marri et al. [6] suggested—actually *increases* the degree of crushing during shear, although the crushing is localised and concentrated around the shear plane. This proposition is supported by the fact that Marri et al. [6] based their suggestion on the perhaps subjective interpretation of images, and the fact that the images themselves were non-intrusive, and did not reveal interior micro scale behaviour. Increasing the degree of cementation/cement content in the simulations (by increasing the quantity of parallel bonds) increases not only the number of overall breakages but also

the percentage of mass of the original material that undergoes breakage; with 1.13, 2.36, 2.96 and 4.18 % by mass of the original samples undergoing crushing in the simulations with averages of 0, 5, 10 and 15 bonds per particle respectively. However, the introduction of crushing does not largely affect the overall stress–strain behaviour of the cemented sand, at least at a confining pressure of 1 MPa.

The observation here that increasing the degree of cementation *increases* the amount of crushing during shear may seem somewhat contrary to the conclusions from authors' work on one-dimensional compression [20]—in which cementation was shown to *decrease* the amount of crushing for a given applied stress. The principal difference it seems, is that during the stress-controlled one-dimensional compression simulations, the cemented sand could exhibit deformation in only one direction (the *z*-axis); during the strain-controlled triaxial simulations the specimens could deform freely in all three directions. If one analyses the actual failure of the triaxial specimens, it can be seen that increasing the quantity of bonds rendered the material more brittle, and *changed* the method of deformation/failure mode. A high level of cementation resulted in localized failure in the form of a shear plane (regardless of whether the particles could break or not); across which parallel bonds broke as the macroscopic strain was applied. According to classical soil mechanics, a shear plane separates two intact 'blocks' of soil, and after rupture, the soil *only* shears on this plane, which becomes much weaker than the rest of the sample and continues to distort. As shearing only takes place between these two intact blocks, the particles on this plane are subjected to much larger shear stresses than elsewhere in the sample. This can be confirmed by inspecting the internal contact forces between the sand particles, which are displayed in Fig. 9 for both the uncemented and heavily cemented crushable simulations. Figure 9a shows the contact forces on a vertical cutting plane through the uncemented sample at 4% axial strain, and displays a fairly uniform distribution. Figure 9b shows the equivalent for the heavily cemented sample, and reveals both larger contact forces as well as a much more irregular distribution. The localised concentrations of internal forces agree with the shear plane revealed in both Figs. 5b, ii and 8; all of these images giving an identical point of view of the sample. The concentration of shear stresses explains the increased breakage on the shear plane shown in Fig. 8a. If one considers the uncemented crushable simulation, as axial strain is applied to the specimen, there is fairly uniform deformation, resulting in barrelling failure, as indicated by Fig. 7a, i. To accommodate the macroscopic strain, *all* particles are free to move relative to each other; by sliding, rotating and rolling over one another. This means that local shearing takes place throughout the whole sample (on a particle-to-particle scale), and therefore almost all particles are subjected to local shear stresses—however, the individual par-

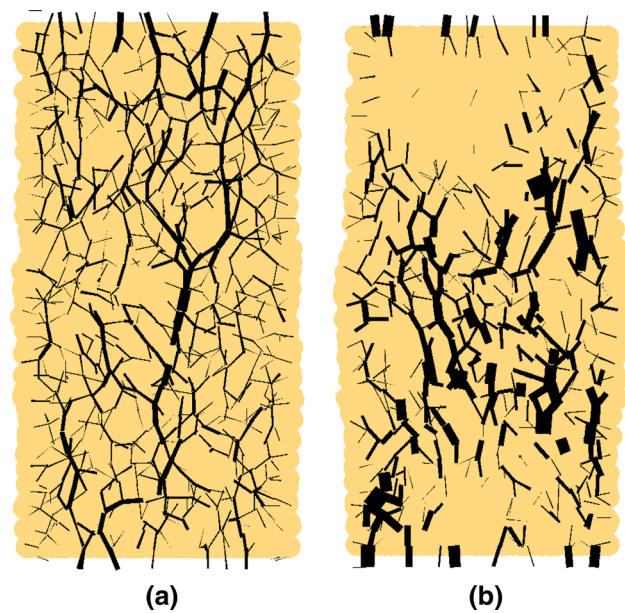


Fig. 9 Images of the uncemented (a) and heavily cemented (b) crushable samples at 4% axial strain, showing the contact forces on the particles on a vertical cutting plane. The thickness of the lines denote the magnitude of each contact force; with maximum forces of 168 and 386 N respectively for the uncemented and cemented samples

ticle stresses will be relatively uniform, and not as high as those on the shear plane in the heavily cemented, brittle material. In the simulations of one-dimensional normal compression by comparison, all samples regardless of cement content exhibited the same mode of failure and deformation, during which, as the applied stress increased, so did *all* the local particle stresses. This is in contrast to the triaxial simulations, in which the bonded particles within the intact 'blocks' were largely not subjected to increasing shear stresses as the test progressed.

4 Conclusions

Sand has been modelled using crushable particles, which break according to the octahedral shear stress induced from multiple contacts, using the mechanism developed by McDowell and de Bono [19]. Cementation has been modelled by incorporating parallel bonds, the presence of which prevented a bonded particle from fracturing. In general, the presence of parallel bonds resulted in the correct qualitative change in behaviour that is observed in laboratory tests, and increasing the degree of cementation—by increasing the quantity of bonds—magnified these effects. The most heavily cemented material resulted in the most brittle failure, with a clear shear plane visible, which was manifested in the location of broken fragments, broken parallel bonds, and the particle rotations. In the cemented material, an *increase* in the degree of crushing was observed with increasing cement con-

tent, with this observation attributed to the change in deformation and failure from ductile to brittle; particle breakage appeared localised and concentrated internally on the failure plane, further highlighting the importance of using a flexible boundary.

Acknowledgments The authors are grateful to the Engineering and Physical Sciences Research Council (EPSRC) for their financial support through the Doctoral Training fund.

References

1. Coop, M.R., Atkinson, J.H.: The mechanics of cemented carbonate sands. *Géotechnique* **43**, 53–67 (1993)
2. Huang, J.T., Airey, D.W.: Properties of artificially cemented carbonate sand. *J. Geotech. Geoenviron. Eng.* **124**, 492–499 (1998)
3. Schnaid, F., Prietto, P.D.M., Consoli, N.C.: Characterization of cemented sand in triaxial compression. *J. Geotech. Geoenviron. Eng.* **127**, 857–868 (2001)
4. Asghari, E., Toll, D.G., Haeri, S.M.: Triaxial behaviour of a cemented gravely sand, Tehran alluvium. *Geotech. Geol. Eng.* **21**, 1–28 (2003)
5. Haeri, S.M., Hosseini, S.M., Toll, D.G., Yasrebi, S.S.: The behaviour of an artificially cemented sandy gravel. *Geotech. Geol. Eng.* **23**, 537–560 (2005)
6. Marri, A., Wanatowski, D., Yu, H.S.: Drained behaviour of cemented sand in high pressure triaxial compression tests. *Geomech. Geoenviron. Eng.* **7**, 159–174 (2012)
7. Hardin, B.O.: Crushing of soil particles. *J. Geotech. Eng.* **111**, 1177–1192 (1985)
8. Yamamuro, J.A., Lade, P.V.: Drained sand behavior in axisymmetric tests at high pressures. *J. Geotech. Eng.* **122**, 109–119 (1996)
9. Jiang, M., Leroueil, S., Konrad, J.: Yielding of microstructured geomaterial by distinct element method analysis. *J. Eng. Mech.* **131**, 1209–1213 (2005)
10. Jiang, M., Yu, H., Leroueil, S.: A simple and efficient approach to capturing bonding effect in naturally microstructured sands by discrete element method. *Int. J. Numer. Methods Eng.* **69**, 1158–1193 (2007)
11. Wang, Y.H., Leung, S.C.: Characterization of cemented sand by experimental and numerical investigations. *J. Geotech. Geoenviron. Eng.* **134**, 992–1004 (2008)
12. Utili, S., Nova, R.: DEM analysis of bonded granular geomaterials. *Int. J. Numer. Anal. Methods Geomech.* **32**, 1997–2031 (2008)
13. Camusso, M., Barla, M.: Microparameters calibration for loose and cemented soil when using particle methods. *Int. J. Geomech.* **9**, 217–229 (2009)
14. Potyondy, D.O., Cundall, P.A.: A bonded-particle model for rock. *Int. J. Rock Mech. Min. Sci.* **41**, 1329–1364 (2004)
15. Wang, Y., Tonon, F.: Modeling triaxial test on intact rock using discrete element method with membrane boundary. *J. Eng. Mech.* **135**, 1029–1037 (2009)
16. Bolton, M.D., Nakata, Y., Cheng, Y.P.: Micro- and macro-mechanical behaviour of DEM crushable materials. *Géotechnique* **58**, 471–480 (2008)
17. Lim, W.L., McDowell, G.R.: The importance of coordination number in using agglomerates to simulate crushable particles in the discrete element method. *Géotechnique* **57**, 701–705 (2007)
18. De Bono, J., McDowell, G., Wanatowski, D.: Discrete element modelling of a flexible membrane for triaxial testing of granular material at high pressures. *Géotech. Lett.* **2**, 199–203 (2012)
19. McDowell, G.R., de Bono, J.P.: On the micro mechanics of one-dimensional normal compression. *Géotechnique* **63**, 895–908 (2013)
20. De Bono, J.P., McDowell, G.R.: Discrete element modelling of one-dimensional compression of cemented sand. *Granul. Matter.* **16**, 79–90 (2013)
21. Itasca: Particle Flow Code in 3 Dimensions. Itasca Consulting Group Inc, Minneapolis (2005)
22. Harireche, O., McDowell, G.R.: Discrete element modelling of yielding and normal compression of sand. *Géotechnique* **52**, 299–304 (2002)
23. Åström, J.A., Herrmann, H.J.: Fragmentation of grains in a two-dimensional packing. *Eur. Phys. J. B.* **5**, 551–554 (1998)
24. Tsoungui, O., Vallet, D., Charmet, J.: Numerical model of crushing of grains inside two-dimensional granular materials. *Powder Technol.* **105**, 190–198 (1999)
25. Lobo-Guerrero, S., Vallejo, L.E.: Crushing a weak granular material: experimental numerical analyses. *Géotechnique* **55**, 245–249 (2005)
26. Ben-Nun, O., Einav, I.: The role of self-organization during confined comminution of granular materials. *Philos. Trans. A. Math. Phys. Eng. Sci.* **368**, 231–47 (2010)
27. Ben-Nun, O., Einav, I., Tordesillas, A.: Force attractor in confined comminution of granular materials. *Phys. Rev. Lett.* **104**, 108001 (2010)
28. McDowell, G.R., Harireche, O.: Discrete element modelling of soil particle fracture. *Géotechnique* **52**, 131–135 (2002)
29. Cheng, Y.P., Bolton, M.D., Nakata, Y.: Crushing and plastic deformation of soils simulated using DEM. *Géotechnique* **54**, 131–141 (2004)
30. Bowman, E.T., Soga, K., Drummond, W.: Particle shape characterisation using Fourier descriptor analysis. *Géotechnique* **51**, 545–554 (2001)
31. Jaeger, J.C.: Failure of rocks under tensile conditions. *Int. J. Rock Mech. Min. Sci. Geomech. Abstr.* **4**, 219–227 (1967)
32. McDowell, G.R., Bolton, M.D.: On the micromechanics of crushable aggregates. *Géotechnique* **48**, 667–679 (1998)
33. McDowell, G.R., Amon, A.: The application of weibull statistics to the fracture of soil particles. *Soils Found* **40**, 133–141 (2000)
34. McDowell, G.R.: On the yielding and plastic compression of sand. *Soils Found* **42**, 139–145 (2002)
35. De Bono, J.P., McDowell, G.R., Wanatowski, D.: Modelling Cemented Sand using DEM. *Advances in Transportation Geotechnics II*. Taylor and Francis, Sapporo (2012)
36. Ashby, M.F., Jones, D.R.: *Engineering Materials 2: An Introduction to Microstructures, Processing and Design*. Pergamon Press, New York (1986)
37. McDowell, G.R., de Bono, J.P., Yue, P., Yu, H.-S.: Micro mechanics of isotropic normal compression. *Géotech. Lett.* **3**, 166–172 (2013)
38. McDowell, G.R., de Bono, J.P.: A new creep law for crushable aggregates. *Géotech. Lett.* **3**, 103–107 (2013)